ACS APPLIED BIO MATERIALS

www.acsabm.org Article

Stimuli Responsive Molecular Exchange of Structure Directing Agents on Gold Nanobipyramids: Cancer Cell Detection and Synergistic Therapeutics

Nishant Kumar Jain,[$] Shubham Pallod,[$] Berney Peng, Rohini Kumari, Deepak Singh Chauhan, Mukesh Dhanka, Eaint Honey Aung Win, Michael A. Teitell, Pranjal Chandra,* Rohit Srivastava,* and Rajendra Prasad*

Cite This: *ACS Appl. Bio Mater.* 2024, 7, 4542−4552 Read Online

ACCESS | Metrics & More | Article Recommendations | Supporting Information

ABSTRACT: Surface-engineered gold nanoparticles have been considered as versatile systems for theranostics applications. Moreover, surface covering or stabilizing agents on gold nanoparticles especially gold nanobipyramids (AuNBPs) provides an extra space for cargo molecules entrapment. However, it is not well studied yet and also the preparation of AuNBPs still remains dependent largely on cetyltrimethylammonium bromide (CTAB), a cytotoxic surfactant. Therefore, the direct use of CTAB stabilized nanoparticles is not recommended for cancer theranostics applications. Herein, we address an approach of dodecyl ethyl dimethylammonium bromide (DMAB) as biocompatible structure directing agent for AuNBPs, which also accommodate anticancer drug doxorubicin (45%), an additional chemotherapeutics agent. Upon near-infrared light (NIR, 808 nm) exposure, engineered AuNBPs exhibit (i) better phototransduction (51 °C) due to NIR absorption ability (650−900 nm), (ii) photo triggered drug release (more than 80%), and (iii) synergistic chemo-phototherapy for breast cancer cells. Drug release response has been evaluated in tumor microenvironment conditions (84% in acidic pH and 80% at high GSH) due to protonation and high affinity of thiol binding with AuNBPs followed by DMAB replacement. Intracellular glutathione (GSH, 5−7.5 mM) replaces DMAB from AuNBPs, which cause easy aggregation of nanoparticles as corroborated by colorimetric shifts, suggesting their utilization as a molecular sensing probe of early stage cancer biomarkers. Our optimized recipe yield is monodisperse DMAB-AuNBPs with ∼90% purity even at large scales (500 mL volume per batch). DMAB-AuNBPs show better cell viability (more than 90%) across all concentrations (5−500 ug/mL) when directly compared to CTAB-AuNBPs (less than 10%). Our findings show the potential of DMAB-AuNBPs for early stage cancer detection and theranostics applications.

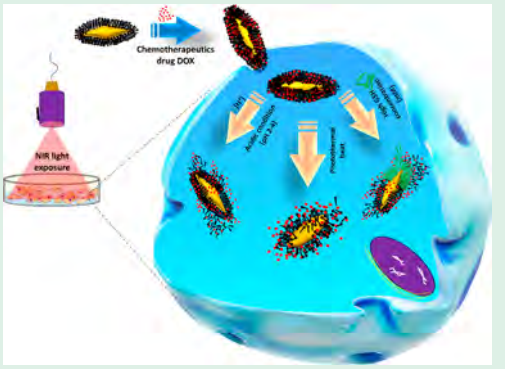

KEYWORDS: *plasmonic nanoparticles, nanobipyramids, cancer cell detection, bioimaging, synergistic therapeutics, drug delivery*

INTRODUCTION

Recent advancements in cancer treatment have focused on targeted therapies, theranostics, and tracking of disease stages using multifunctional nanoparticles.[1−11] Much of this research is devoted to the utilization of elongated plasmonic metal nanostructures, such as gold nanorods, to image and treat tumors using photothermal therapy (PTT), a noninvasive technique that uses the absorbance of NIR light to locally ablate tumors with heat.[12−15] This treatment approach is clinically known as hyperthermia. To the best of our knowledge, the plasmonic nanoparticles have been tried for light mediated tumor therapy in clinical applications. Especially metal nanomaterials such as gold exhibit localized surface plasmon resonance (LSPR) that stems from a collective oscillation of conduction band electrons.[9,12,16] This enables the strong absorbance of specific wavelengths of light and leads to a strong extinction band at around 800 nm in colloidal gold nanorod (AuNRs) solutions.[1−4] Changes in particle size, aggregation, or morphology can further alter nanomaterial optical and photothermal properties.[16−18] This is an especially attractive feature for PTT applications, as NIR light produces lower scattering and higher tissue penetration following irradiation, resulting in more efficient *in vivo* heating.[1,3−5,19] Moreover, gold nanomaterials are biocompatible and are easily surface-functionalized with antibodies or drug molecules.[1,3−5]

Received: March 25, 2024
Revised: June 20, 2024
Accepted: June 21, 2024
Published: July 3, 2024

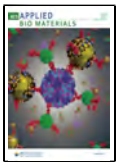

https://doi.org/10.1021/acsabm.4c00409
ACS Appl. Bio Mater. 2024, 7, 4542−4552

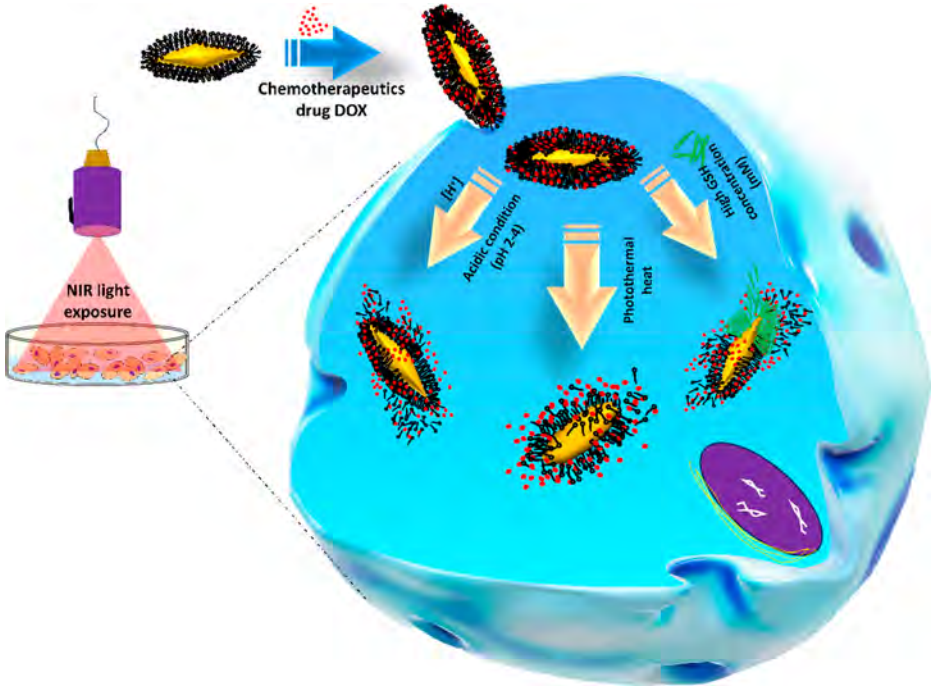

Figure 1. Schematic representation showing stimuli responsive molecular exchange of structure directing agents on gold nanobipyramids within cancer cell interior.

To the best of our knowledge, different shapes of nanoparticles viz., gold nanorods, nanobipyramids, and nanoshell/auroshell could induce similar levels of temperature elevation upon same energy and LSPR conditions. However, these nanoparticles may produce different levels of reactive oxygen species (ROS), which is equally important to destroy the cancer cells.

Especially, gold nanobipyramids (AuNBPs) possess advantages over other types of gold nanostructures as they exhibit facile synthesis, large local electric field enhancements, high optical cross sections, and narrow line widths, resulting in more desirable optical properties for bioimaging.[3,5,15] Synthesized nanobipyramids are remarkably monodisperse with a full-width half-max (fwhm) ranging from 50 to 100 nm, which is much lower than gold nanorods.[20,21] The quantum yield of bipyramids is also comparatively higher because of additional field enhancement at the tips.[22] Moreover, the LSPR wavelength of gold nanobipyramids (AuNBPs) is easily tunable by changing seed concentration,[23] and AuNBPs also exhibit significantly higher photoluminescence than gold nanorods.[24] High-purity solutions of gold nanoparticles and AuNBPs have been shown to possess many applications in diagnostics, therapeutics, sensing, and energy storage.[1−5,12−15] For instance, precise assessment of cancer cell interior conditions (high level of GSH, acidic pH) using gold nanoparticles not only is favorable for pathophysiological understanding but also indicate diseases diagnosis at early stage. However, affordable and early stage cancer cell detection approaches yet to be achieved. On the other hand, Wu et al. demonstrated the use of gold nanoparticles viz., AuNBPs in photothermal therapy against cancer cells while monitoring local temperatures.[20] AuNBPs were coated with short fluorophore-tagged DNA hairpin structures, which opened upon incidence of NIR light, leading to an increase in fluorescence, and the heating of AuNBPs led to cancer cell death.[20] Although AuNRs and AuNBPs have been shown to be effective theranostic agents, their synthesis involves the use of toxic cationic surfactants, CTAB or cetyltrimethylammonium chloride (CTAC), to obtain high purities.[21] In a study by Chateau et al., gold seeds were prepared in the presence of CTAC as opposed to CTAB or citrate.[25] This study demonstrated that CTAC as well as CTAB can promote the formation of very high aspect ratio structures, nanojavelins, that possess NIR LSPR wavelengths.[25] However, for the successful translation of nanomedicines to clinical applications, it is essential that synthesized materials are physiologically biocompatible. Herein, we aimed to synthesize more biocompatible AuNBPs using DMAB, which has been previously identified as a biocompatible surfactant alternative to CTAB and CTAC.[21] CTAB stabilized AuNBPs are popular but have significant toxicity issues. Hence, the direct use of CTAB-stabilized NBPs is not recommended for biomedical applications.

In this study, we have prepared AuNBPs followed by a seed-mediated method using sodium borohydride, a mild reducing agent for the reduction of chloroauric acid.[26−36] In brief, the reaction is carried out in the presence of citrate, which caps and stabilizes the seeds. Citrate also helps in twinning defects and polycrystallinity in the seeds which promote AuNBPs formation.[33] The growth solution for the synthesis consists of chloroauric acid reduction by ascorbic acid. We have used dodecyl ethyl dimethyl ammonium bromide (DMAB) as biocompatible structure directing agent instead of toxic CTAB. DMAB provides a soft template for the growth of seeds. Silver nitrate is added to the solution as a shape-directing agent. During AuNBPs preparation, we find that the crystallinity of seeds is the most crucial parameter that determines the shape of the grown structure. Polycrystalline and decahedral seeds are found to produce bipyramidal structures, while monocrystalline seeds produce nanorods. From various optimizations, we have noticed that AuNBP exhibit reduced LSPR wavelength in the case of increasing seed volume and low pH. Maximum purity (greater than 90%) and optically stable

https://doi.org/10.1021/acsabm.4c00409
ACS Appl. Bio Mater. 2024, 7, 4542−4552

(more than 25 days) AuNBPs have been obtained while using heated seeds in the presence of citrate. To gain insights into how well CTAB-free AuNBPs perform (i) carrying extra cargo (doxorubicin anticancer drug named as DOX), (ii) photo-transduction response, (iii) photo triggered synergistic chemo-phototherapeutics response, and (iv) sensing biomolecules related to cancer cells viz., GSH, we have conducted microscopic and spectroscopic examinations. We have understood that dense network of DMAB structure directing agents over AuNBPs helps in accommodating excess anticancer drug doxorubicin (45% calculated based on spectroscopic measurements), which is further released in cancer mimicked environment (low pH and high GSH level) in terms of therapeutics response. Upon near-infrared light (NIR, 808 nm) exposure, drug entrapped AuNBPs exhibit photo triggered cancer cell death (more than 85%) due to synergetic effect of generated heat (51 °C) and released anticancer drug. Additionally, upon GSH (5−7.5 mM) interaction DMAB-AuNBPs demonstrate rapid aggregation and morphology deformation due to competitive replacement between GSH and DMAB, which is further corroborated by spectroscopic and microscopic validations. These observations indicate the importance of AuNBPs as molecular sensor for early stage detection of cancer biomarkers. Better reproducibility (more than 15 times) and scalability (500 mL volume per batch) are the key aspects of our optimized recipe.

RESULTS AND DISCUSSION

Gold Nanobipyramids (AuNBPs) and Their Interface. Plasmonic nanoparticles, viz., AuNBPs were synthesized using a modified seed-mediated method with biocompatible DMAB as a structure-directing agent as shown in Scheme S1 in the Supporting Information (SI). Figure 1 shows the stimuli responsive molecular exchange of structure directing agents on drug entrapped gold nanobipyramids within cancer cell interior. As an initial step, gold seeds were prepared by reducing $HAuCl_4$ with $NaBH_4$ in either the presence of CTAC and citric acid (heated) or citrate (unheated). The morphology and optical property of unheated seed showing orange color was characterized by TEM and UV−vis spectrum as shown in SI, Figure S1. Following at least 2 h of aging at 30 °C, the prepared gold seeds were introduced to a growth solution containing $HAuCl_4$, $AgNO_3$, HCl, and DMAB. A mild reducing agent, ascorbic acid, was added to the stirred solution, changing the color of the solution from light yellow to colorless (see Materials and Methods section and Supporting Information). TEM image analysis of gold seeds displayed the presence of multitwinned nanostructures of size ∼5 nm (SI, Figure S1). The addition of 85 μL of unheated gold seed solution to the growth solution initiated the NBP formation. DMAB structure directing agents stabilized gold nanoparticles exhibit perfect bipyramids dimension (∼100 nm length and ∼32 nm diameter, aspect ratio of 3.1), validated through TEM imaging as shown in Figure 2. Prepared DMAB stabilized gold nanobipyramids show similar morphology, size, aspect ratio (3.1), and optical property as widely reported for CTAB stabilized gold nanobipyramids (see Figure 2 and Figure 3a−e). Thick deposition of DMAB around AuNBPs indicate their dense self-assembly due to double-chain cationic nature, which stabilize these gold nanoparticles for prolonged time and also entrap extra cargo molecules to demonstrate multimode imaging and therapeutics individually or in combination, whereas a single-chain cationic surfactant like CTAB makes fewer stable bilayers around the AuNBPs.

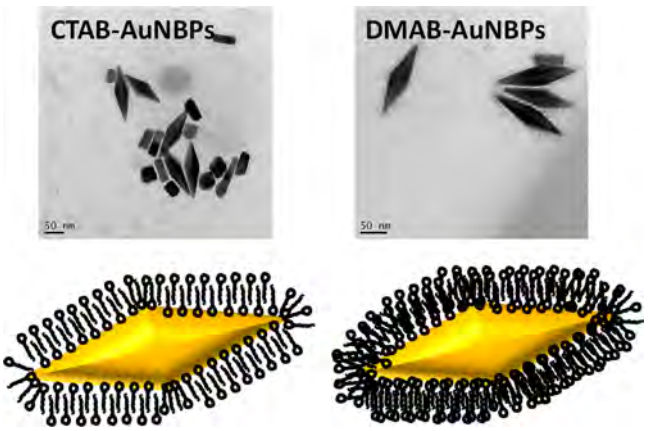

Figure 2. Microscopic images for surface interfaces examination of CTAB and DMAB stabilized AuNBP obtained from seed mediated growth procedure.

Feret diameter measurements quantified from image analysis verified comparable size distributions between the two synthesis approaches, with longitudinal diameters determined between 90 and 100 nm (SI, Figure S2). Violin plots show that DMAB-AuNBP sizes may be more monodispersed than CTAB-AuNBPs. The aspect ratio of both DMAB and CTAB AuNBPs was observed around 3. In absorption spectroscopic measurements, these surface-engineered plasmonic nanoparticles showed two distinct characteristic peaks, viz., transverse (∼540 nm) and longitudinal (∼800 nm), indicating their localized surface plasmon resonance (LSPR). We noticed that both DMAB stabilized AuNBPs and CTAB stabilized AuNBPs displayed similar absorbance spectra overall. The relatively sharp full width at half-maximum (fwhm) at the 800 nm NIR peak (Figure 3c) for both DMAB- and CTAB-fabricated AuNBPs denotes the formation of uniformly sized particles. Like the TEM images, the absorbance data further illustrates that, apart from NBPs, irregular nanospheres and their aggregates were also present in solution for both synthesis approaches. The approximate purity of NBPs was estimated by comparing the LSPR peak absorption of NBPs to the characteristic absorption of spherical impurities at ∼560 nm.[37]

DMAB-directed seed-mediated synthesis produced AuNBPs in solution with a purity of ∼45% (Figure 3c inset: digital photograph of seed solution). Removal of these undesired particles in solution is necessary to increase AuNBP yields. The colloidal stability of DMAB-AuNBPs was monitored with UV−vis spectroscopic measurements by observing shifts ∼800 nm LSPR peak position over time. DMAB-AuNBPs were colloidally stable over 25 days of observation, retaining their LSPR absorption peak for the entire duration and showing only slight blue-shifting by day 25 (Figure 3f).

Optimization and Purity of AuNBPs. Purity, morphology, and optical properties of DMAB stabilized AuNBPs using unheated seed-mediated synthesis were tightly controlled by DMAB concentration, pH as adjusted by HCl, and gold seed volume addition to the growth solution. The position of the NBP LSPR peak was dependent upon particle aspect ratio, where higher aspect ratio particles exhibit higher LSPR wavelengths. In the DMAB-AuNBP unheated seed approach, different volumes of gold seed solution ranging from 60 to 140 μL were added to the growth solution. The morphology and

https://doi.org/10.1021/acsabm.4c00409
ACS Appl. Bio Mater. 2024, 7, 4542−4552

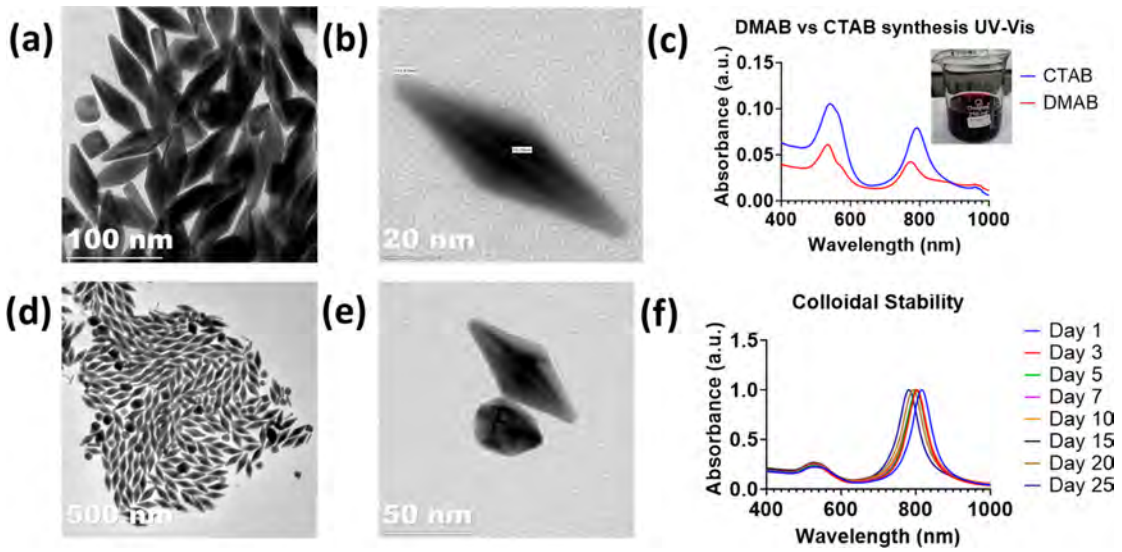

Figure 3. Characterization of DMAB and CTAB-directed AuNBP synthesis. (a,b) FEG-TEM (300 keV) images of DMAB-AuNBPs synthesized with unheated seeds. The longitudinal axis of the NBPs is ∼100 nm. (d,e) FEG-TEM (300 keV) images of AuNBPs synthesized from traditional CTAB methods. (c) Comparison of UV−vis spectra of DMAB and CTAB-synthesized AuNBPs. The digital inset depicts a colored solution of DMAB-AuNBPs. DMAB-AuNBPs show similar purities and optical properties as the CTAB-directed growth particles. (f) Stability of purified DMAB-AuNBPs demonstrated via normalized UV−vis spectra over 25 days.

optical properties of prepared AuNBPs were examined through microscopic imaging (Figure 4) and spectroscopic measurements (Figure 5a).

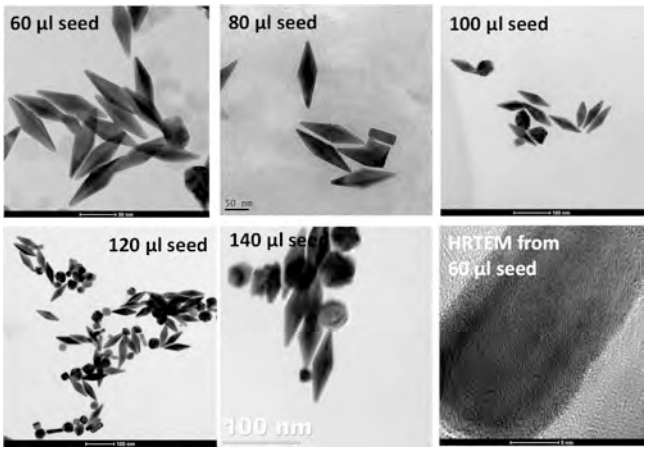

Figure 4. TEM images of prepared AuNBPs using different seed volumes (60−140 μL) and high-resolution TEM image (HRTEM) of AuNBPs.

When higher seed volumes were added, the LSPR peak wavelength blue-shifted from 876 to 796 nm. Lower concentrations of Au growth solution relative to initial seed density (because higher amounts of seed were added) in the reaction mixture led to the formation of NBPs with lower aspect ratios. The converse appeared to be true for higher gold growth solution concentrations per seed. The LSPR wavelength and ratio of absorptions at LSPR wavelength and wavelength pertaining to spherical impurities as a function of seed volume are tabulated in Table 1. While the purity of DMAB-AuNBPs was similar across all DMAB concentrations in the growth solution, decreasing concentrations of DMAB from 0.3 to 0.05 M red-shifted the longitudinal peak from ∼700 to ∼800 nm (Figure 5b). At a very low (0.025 M) DMAB concentration, the absorbance intensity and location of the longitudinal peak decreased significantly, indicating the presence of impurities and a lower synthesis yield.

The pH of the growth solution was another parameter in which the formation of NBPs and their morphology could be manipulated as the reducing ability of ascorbic acid decreases at low growth solution pH. The pH of the reaction mixture was controlled by HCl volume addition. As more HCl was added to the Au growth solution (from 20 to 200 μL, corresponding to a change in pH of 2.46 to 1.87, respectively), it caused a blue-shift in the LSPR peak (Figure 5c). At higher pH growth conditions, the solution color changed rapidly during the formation of NBPs. In lower pH growth conditions, the solution color changed much slower, illustrating the kinetically limited ability of the reducing agent (Figure 5d). Moreover, at lower pH, the color of the AuNBP solution had a violet hue, and at a higher pH, the color was dark red. When no HCl was added (pH 2.97), the combined growth and seed solution mixture color remained black, and a precipitate at the bottom of the tube was observed after 16 h.

BDAC-mediated depletion flocculation combined with several centrifugation conditions were employed to increase AuNBP purity in solution following DMAB-AuNBP synthesis (Figure 5e,f). The addition of BDAC caused flocculation of both nanospheres and AuNBPs, so AuNBPs could not be selectively precipitated from solution and separated from the nanospheres. This is shown by the presence of both nanosphere and AuNBP peaks following the resuspension of the precipitate in DMAB (Figure 5e). The TEM image in Figure 3f shows little to zero AuNBP purity improvement. DMAB stabilized AuNBPs were also centrifuged without BDAC at varying conditions ranging from 5k to 10k rpm and 5−10 min. Maximum purity was obtained at 5k rpm and 10 min of centrifugation followed by resuspension in DMAB (SI, Figure S3). If too little DMAB was used, the NBPs remained flocculated and could not be fully redispersed.

The formation of NBP structures from seed-mediated growth is heavily influenced by the polycrystallinity of the

https://doi.org/10.1021/acsabm.4c00409
ACS Appl. Bio Mater. 2024, 7, 4542−4552

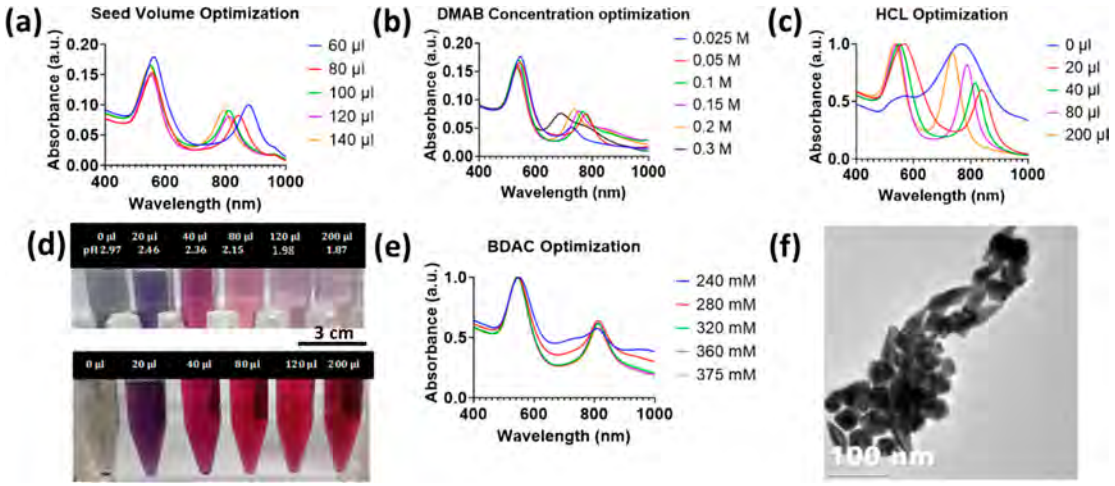

Figure 5. Optimization of reaction conditions for unheated seed-mediated synthesis. (a) UV spectra of nanocrystals prepared using different seed volumes. (b) UV−vis spectrum of as synthesized nanocrystals with different concentrations of DMAB. (c) UV−vis spectrum for pH optimization with HCl addition. (d) Digital photos depicting color changes at different pH and different times (upper, 30 min; lower, 16 h after seed addition). (e) UV spectra of AuNBP solution following purification using benzylhexadecyldimethylammonium chloride (BDAC) depletion flocculation to improve purity. AuNBPs were selectively precipitated out of solution from the spherical nanoparticles and the supernatant was removed. (f) FEG-TEM of AuNBP nanocrystals after their resuspension in water and DMAB following BDAC purification.

Table 1. Effect of Seed Volume on LSPR Wavelength and Purity[a]

seed vol (μL)	LSPR wavelength (nm)	$A_{LSPR}/A_{560\ nm}$
60	876	0.56
80	843	0.54
100	811	0.55
120	811	0.55
140	796	0.56

[a]Increasing the amount of gold seed in the growth solution generated NBPs possessing lower LSPR peak wavelengths.

starting seed material.[29] To increase the yield and purity of AuNBP fabrication, it is essential to increase the proportion of polycrystalline seeds added to the growth solution. To do so, the seeded growth reaction mixture was exposed to high temperatures (85 °C for 1.5 h) in the presence of citrate ions to produce more polycrystalline seeds and promote AuNBP formation with high shape purity. UV−vis spectra of AuNBPs produced from heated seeds showed the characteristic strong ∼800 nm LSPR peak (Figure 6a). The calculated yield was more than 90%. The UV−vis results were corroborated by TEM imaging (Figure 6b), in which high percentages of bipyramidal-shaped nanostructures were observed. The small number of impurities consisted of Au nanospheres and nanorods. Furthermore, AuNBPs synthesized using DMAB can be easily distinguished from those synthesized using CTAB. DMAB-AuNBPs tend to grow individually, whereas CTAB-AuNBPs appear to grow side-to-side, forming array-like structures observed with TEM (Figure 6c). Further, the prepared plasmonic nanoparticles were tested for cancer cell imaging, synergistic chemophototherapy, sensing cancer cell biomarkers, and drug delivery performance as discussed in below sections. A brief comparison of photothermal response of different plasmonic nanoparticles has been highlighted in the Table S1 Supporting Information.

Cancer Cell Detection and Synergistic Therapeutics Response of DOX-AuNBPs. Dodecyl ethyl dimethyl ammonium bromide (DMAB) stabilized AuNBPs nanoparticles were incubated with an anticancer drug doxorubicin which was utilized for cancer cell imaging and chemotherapeutics applications. High drug loading efficiency (45%) was achieved due to decorated DMAB surfactants over AuNBPs, which was purified through dialysis (12 kDa MW cutoff for 1 day). To evaluate the chemotherapeutics response, these DOX entrapped gold nanoparticles were tested for DOX release kinetics pattern at different cellular environment, viz., extracellular (pH 7.4) and intracellular (pH 6−2), as shown in Figure 7a. Within 10 h, significant drug release (more than 90%) DOX release was noticed in acidic environment (pH 2,

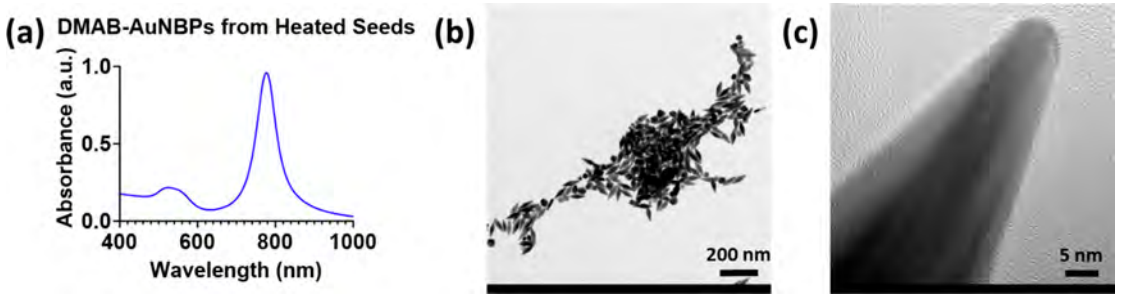

Figure 6. Characterization of AuNBPs synthesized using heated seeds. (a) UV−vis spectrum of synthesized NBPs from heated Au seeds. (b,c) FEG-TEM (300 keV) images of NBPs synthesized using citric acid-containing seeds.

https://doi.org/10.1021/acsabm.4c00409
ACS Appl. Bio Mater. 2024, 7, 4542−4552

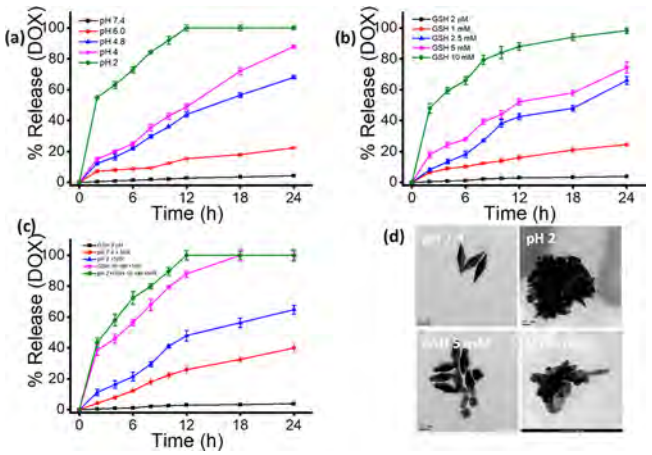

Figure 7. Drug release response of DOX entrapped DMAB-AuNBPs in physiological and cancer therapeutics conditions (a−c) and microscopic images of treated DOX entrapped DMAB-AuNBPs in respective therapeutics stimulus (d).

viz., intracellular environment of cancer cells) as compared to the physiological pH 7.4 (∼2%) due to protonation effect at lower pH (Figure 7a). Further, the maximum DOX release (100%) was noticed within 12 h of incubation at pH 2, whereas ∼49% was achieved for pH 4 in the same time, which were significantly higher to the physiological pH 7.4. In 24 h of kinetics, pH 4 showed maximum 88% of DOX release, which was better than other pH conditions (∼23% for pH 6, and ∼4.5% for pH 7.4). Next, DOX release pattern was also examined in other cancer mimicked condition, viz., different GSH concentrations (1−10 mM). Better DOX release (more than 90%) was noticed at 10 mM GSH as compared to extracellular GSH level (∼4% at 2 μM) in 24 h of incubation. Interestingly, promising DOX release (66−75%) was seen at moderate level of GSH (2.5 and 5 mM) as shown in Figure 7b. Based upon DOX release performances in various conditions, the designed plasmonic nanohybrid demonstrate its suitability for chemotherapeutics application. On the other hand, DOX entrapped gold nanoparticles were also tested for photo triggered drug release upon near-infrared light (NIR, 808 nm) exposure as shown in Figure 7c. Significant DOX release (∼65%) at acidic environment (pH 2) upon NIR light irradiation, which was due to protonation and photothermal disassembly of DMAB on the AuNBPs surface, whereas 40% drug release response was noticed at pH 7.4 during NIR light exposure. It should be noted that negligible drug release response (∼4%) was noticed at physicochemical conditions (pH 7.4 and without NIR light treatment). Moreover, significant drug release (∼90%) was noticed in the case of actual synergistic chemophototherapeutic conditions (pH 2 and 10 mM GSH upon NIR light exposure) as shown in Figure 7c. During synergistic chemophototherapeutic conditions, there was a replacement of DMAB structure directing agents from the AuNBPs surface due to protonation, competitive capping agent exchanges, and produced heat, respectively, showed deformed gold nanoparticles which was examined through microscopic imaging as shown in Figure 7d. Moreover, the morphology changes of nanoparticles in above-mentioned therapeutics conditions ensured the replacement of surface stabilizing agents due to internal stimuli (acidic pH and GSH) and external stimuli (NIR light) as shown in Figure 7d. Further, these observations were corroborated with cancer cell imaging analysis and microscopic imaging resulted the therapeutic response of engineered plasmonic nanoparticles shown in Figure 8. Homogeneous red fluorescence from cancer cell interior indicated the presence of released DOX, which was due to replacement of surface stabilizing agents, viz., DMAB that entrapped the DOX. We observed enhanced fluorescence intensity of released cargo (DOX) with respect to incubation time (from 1 to 12 h). Moreover, released anticancer drug changed the morphology of cancer cells indicated their death, as shown through fluorescence images in Figure 8, whereas nanoparticles treated cancer cells maintain their morphology in physiological environment (pH 7.4, minimum concentration of GSH and without NIR light irradiation). Rapid aggregation and deformation of nanoparticles were observed in therapeutics conditions (acidic pH 2, GSH 7.5 mM, and NIR light irradiation) as shown in transmission electron microscopic images in Figure 8.

Next, the biocompatibility of DMAB-synthesized AuNBPs were compared to CTAB-AuNBPs using *in vitro* cellular cytotoxicity assays. MDA-MB-231 human breast cancer cells and L929 mouse fibroblasts were exposed to AuNBPs at five different concentrations, ranging from 5 to 500 μg/mL. In L929 cells, DMAB-AuNBPs displayed dramatically better biocompatibility (more than 85%) than CTAB-AuNBPs (less than 25%) across all concentrations even at the highest concentration, 500 μg/mL ensured the biocompatibility of DMAB structure directing agents over CTAB surfactant (Figure 9a). To demonstrate theranostics capabilities, DMAB-AuNBPs were integrated with DOX, where DOX was trapped within the layers of DMAB on the surface of AuNBPs.[38,39] DOX is a standard chemotherapy drug used for a variety of cancer treatments, including breast cancer. DOX entrapped DMAB-AuNBP particles showed significantly higher anticancer drug (DOX) response for substantial cancer cell death (∼84%) in elevated acidic conditions (pH 2−4 for cancer cell interior) with quick uptake.[40] When illuminated with NIR light to activate photothermal heating, DOX-DMAB-AuNBP particles showed even higher cancer cell killing (more than 90%) due to synergistic photochemotherapeutics response, viz., photo triggered release of DOX.[41,42] Prior to cancer therapeutics ability of plasmonic nanoparticles, the photothermal profile of DMAB-AuNBPs at four different concentrations was separately evaluated in aqueous solution after irradiation with an 808 nm laser (2 W/cm^2, SI, Figure S4a). Phototransduction response of DMAB-AuNBPs also measured at various power densities (0.5−2.0 W/cm^2) as shown in SI, Figure S4b in the Supporting Information. Greater amounts of DMAB-AuNBPs led to a greater temperature increase, reaching a peak temperature of 51 °C after 4 min of illumination with a 230 ppm AuNBP concentration. The biocompatibility gap was greater when the cell viability of DMAB-AuNBPs was evaluated against CTAB-NBPs in normal fibroblast cells (L929). Again, DMAB-AuNBPs showed very little cellular cytotoxicity for all particle concentrations examined in sharp contrast to CTAB-AuNBPs (Figure 9b). CTAB-AuNBPs appeared to be more harmful to normal L929 cells than the MDA-MB-231 cancer line. To examine cell imaging and uptake, breast cancer cells (MDA-MB-231) were treated with DOX-DMAB-AuNBPs at different incubation time points (starting from 1 to 12 h). Confocal fluorescent imaging showed the rapid *in vitro* uptake of DOX-DMAB-AuNBPs in MDA-MB-231 cells within 1 h, which was

https://doi.org/10.1021/acsabm.4c00409
ACS Appl. Bio Mater. 2024, 7, 4542−4552

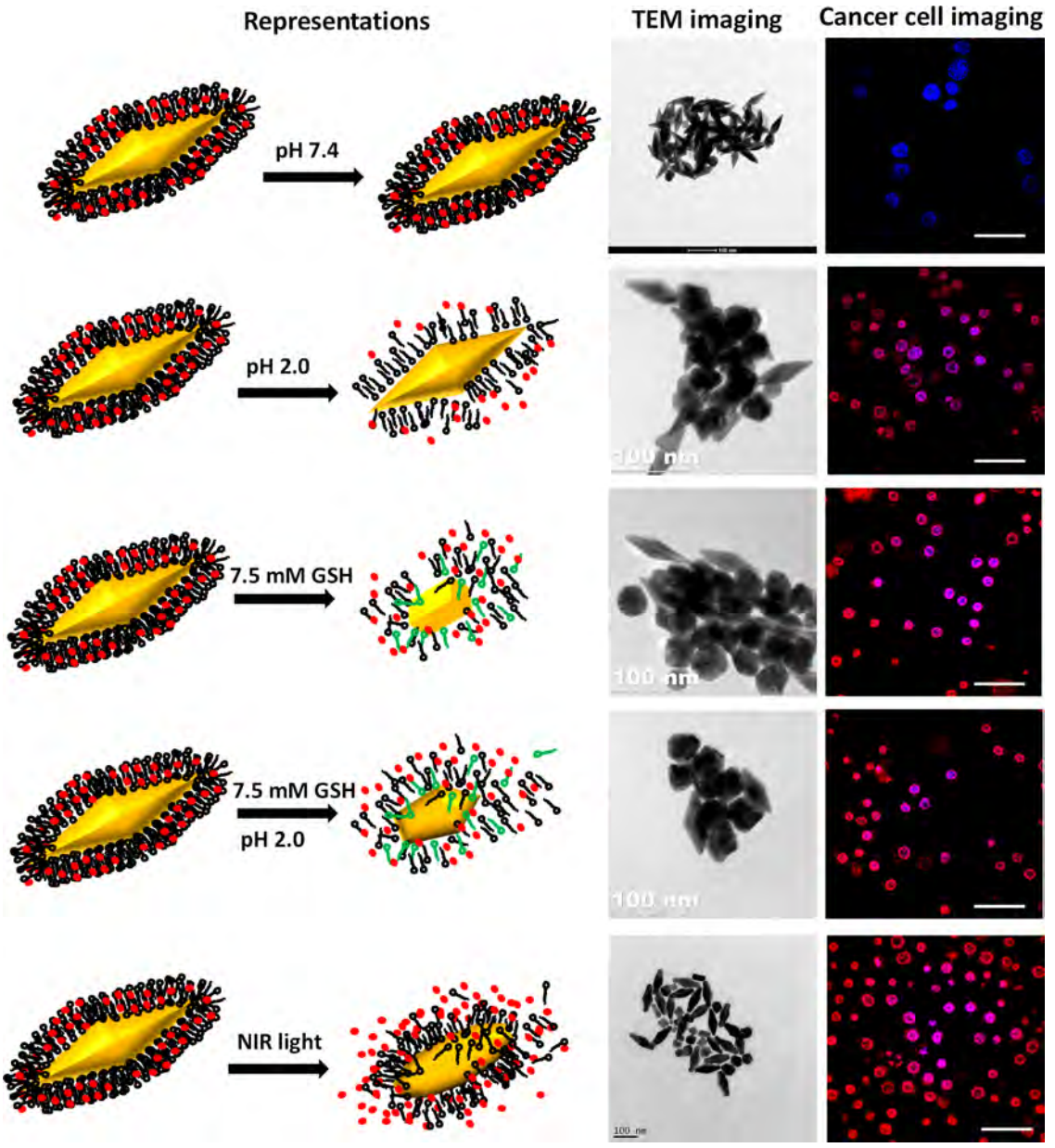

Figure 8. Drug entrapped gold nanobipyramids for cancer cell detection and synergistic chemophototherapeutics upon photo triggered and tumor microenvironment conditions corroborated with transmission electron microscopic and cancer cell (60×) imaging.

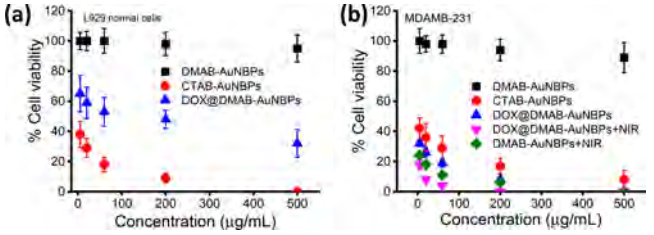

Figure 9. Concentration dependent *in vitro* cell biocompatibility (a), and synergistic chemophototherapeutics, chemotherapeutics, and phototherapeutics response (b) of engineered gold nanobipyramids (with and without drug entrapment) upon photo triggered and tumor microenvironment conditions.

significantly higher in 12 h of incubation (see Figure S5 and Figure S6 in the Supporting Information).

AuNBPs for Glutathione Detection at Molecular Level. The high level of GSH (a few tens in mM) is a remarkable hallmark for cancer cells, which is several hundred times higher than healthy cells. The high concentration of GSH reduces (10−20 mM) the chemotherapeutic and radiation therapeutic effects in solid tumors due to its reactive oxygen species scavenging ability. Therefore, detecting GSH is considered an essential need for examining cancer cells at an early stage. However, the present approach for measuring GSH level involves cellular extraction, which is not a precise method to evaluate GSH. Among various nanoparticles, gold nanoparticles have previously been used as GSH detection. Exposure to GSH causes gold nanoparticle aggregation due to rapid exchange between existing surfactant on the surface of nanoparticles and excess GSH in the medium, leading to color change in colloidal solutions and absorption shifts.[34,35] Hence, we utilized newly designed gold nanoparticles, viz., AuNBPs to

https://doi.org/10.1021/acsabm.4c00409
ACS Appl. Bio Mater. 2024, 7, 4542−4552

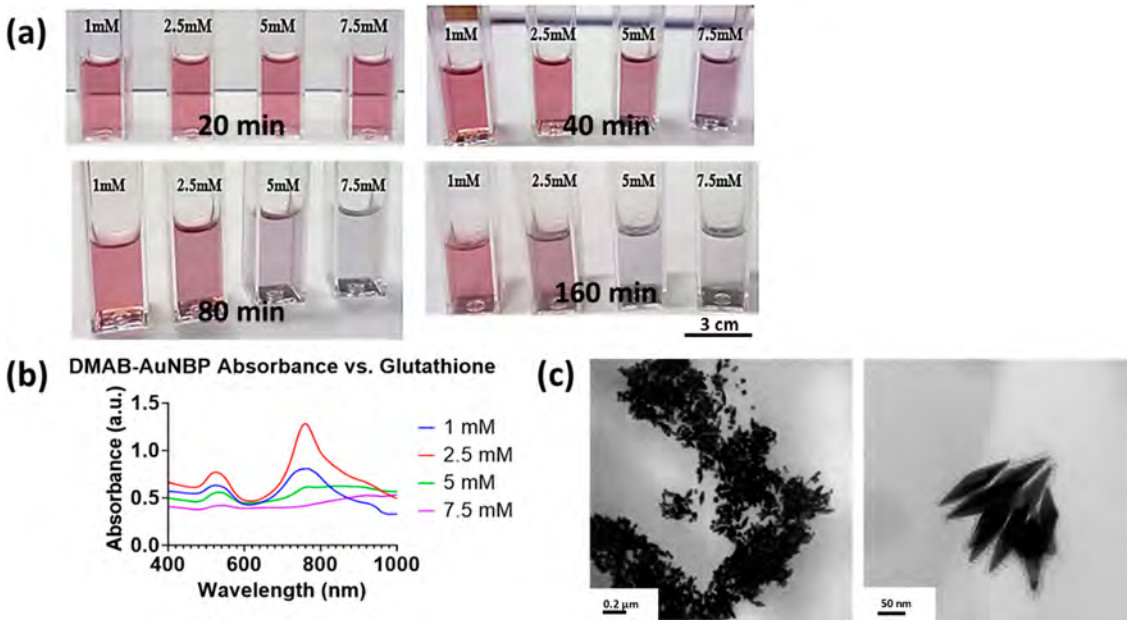

Figure 10. Molecular GSH response of AuNBPs. (a) Digital photographs showing color change for different GSH concentrations with respect to time. (b) UV−vis−NIR spectra of DMAB-AuNBPs in solution after 80 min of immersion with 1, 2.5, 5, and 7.5 mM of glutathione. (c) HR-TEM (300 kV) image of aggregated NBPs in the presence of 5 mM glutathione (left) and saline control (right).

detect GSH at molecular level within cancer mimicked conditions. To test this, high concentrations of GSH (cancer cell interior condition GSH in mM range) were added to DMAB-AuNBPs in solution, altering the native reddish color of the solution progressively to essentially colorless over time (Figure 10a). Four different concentrations (1, 2.5, 5, and 7.5 mM) were tested (Figure 10a, and SI, Figure S7), which is consistent with physiological levels of GSH found in the cytosol of cells (1−10 mM).[36] The time it took to change the color depended on GSH concentration, and eventually, all DMAB-AuNBP solutions became colorless and formed a black precipitate at the bottom regardless of the initial GSH concentration. The 7.5 mM GSH condition exhibited the fastest color change, while the slowest change was observed at 1 mM GSH. Figure 10b displays the corresponding spectral change in UV−vis absorbance as a function of time and GSH concentration. The UV−vis spectra at high GSH amounts show a gradual flattening of spectra over time, corresponding to the loss of color. DMAB-AuNBPs were suspended in saline as a control. TEM imaging showed little aggregation in the saline solution (Figure 10c, right) and substantial aggregation in the 5 mM GSH solution (Figure 10c, left).

CONCLUSION

Gold nanoparticles are well studied and reported in the literature; however, their dual response is less explored. In this study, we have investigated the preparation of AuNBPs using dodecyl ethyl dimethyl ammonium bromide (DMAB) as a structure directing agent which improves the biocompatibility and cargo capacity of engineered AuNBPs. These DMAB stabilized AuNBPs exhibit monodispersed morphologies similar to CTAB-directed AuNBPs with better yields (90%) at ever reported large scales (500 mL/batch). Optical and morphological characteristics are validated through spectroscopic and microscopic examinations, respectively. Due to better surface plasmon resonance and heat response (51 °C), these particles demonstrate photo triggered drug release (more than 80%) and synergistic chemophototherapy for breast cancer cells under near-infrared light (NIR, 808 nm) irradiation. We have noted significant drug release response (66−74%) in tumor microenvironment conditions. Interestingly, the observed aggregation of plasmonic nanoparticles indicating the rapid exchange between excess glutathione and DMAB surfactant over AuNBPs's surface within cancer mimicked environment. Hence, it is an indication of detecting cancer cell related biomarkers at molecular level for early stage cancer diagnosis. Overall, we have investigated a reliable synthesis recipe (more than 15 times) of biocompatible plasmonic nanoparticles, demonstrating multifunctional response for cancer theranostics applications.

MATERIALS AND METHODS

Materials. Gold chloride trihydrate ($HAuCl_4{\cdot}3H_2O$) ≥99.9% (Sigma), sodium citrate tribasic dihydrate ≥99.0% (Merck), sodium borohydride ($NaBH_4$) 98.0% (Merck), 35% hydrochloric acid (HCl) (SRL), cetyltrimethylammonium bromide (CTAB) ≥99% (Sigma), dodecylethyldimethylammonium bromide (DMAB) ≥98.0% (Sigma), benzenedimethylhexadecylammonium chloride (BDAC) (Sigma), silver nitrate ($AgNO_3$) (SRL), cetyltrimethylammonium chloride (CTAC) (TCI chemicals) >95.0%, citric acid (SRL) 99.5%, and reduced glutathione (GSH) (SRL) 99%.

Methods. *Synthesis of AuNBPs.* CTAB-free AuNBPs were synthesized using the seed-mediated growth method. To prepare gold seeds, $HAuCl_4$ (10 mM, 125 μL) and sodium citrate (10 mM, 250 μL) were added in 9.625 mL of deionized water. The solution was stirred for 1 min. Ice-cold $NaBH_4$ (0.01 M, 150 μL) was slowly added to the solution, after which the color of the solution turned reddish orange, indicating the formation of gold seeds. The seeds were left to age for at least 2 h at 30 °C. For growth, AuNBPs were synthesized by a seed-mediated method. The seed solution was prepared by a constant heating protocol. In brief, 4 mL of $HAuCl_4$ was added to a 4 mL, 95 mM CTAC solution. Then 100 μL of ice-cold $NaBH_4$ was quickly added to the solution. The solution was stirred for 1 min to allow the release of H_2 gas. Citric acid (160 μL, 0.1M) was added to the solution. The vial was tightly capped and heated at 85 °C for 1.5 h.

https://doi.org/10.1021/acsabm.4c00409
ACS Appl. Bio Mater. 2024, 7, 4542−4552

Synthesis of Biocompatible AuNBPs. The preparation of seed was the same as mentioned earlier. Here, biocompatible surfactant DMAB was used to prepare the growth solution; $HAuCl_4$ (0.01 M, 200 μL), $AgNO_3$ (0.01 M, 40 μL), and HCl (1N, 80 μL) were added to a 4 mL, 0.1 M DMAB solution. The solution was stirred, and ascorbic acid (0.1M, 32 μL) was added to the vial. After the addition of ascorbic acid, the color of the solution changed from light yellow to colorless. In this solution, 85 μL of seed solution were added to initiate the nanostructure formation process. The solution was incubated at 30 °C for 4 h. The color of the solution gradually changed from colorless to red. The solution was then centrifuged at 5000 rpm for 10 min. The supernatant was discarded, and the pellet was quickly resuspended in 4 mL of 10 mM DMAB for further processing. Further, purified nanoparticles were studied by various characterizations. The UV−vis−NIR spectrum of synthesized AuNBP solutions were analyzed from 400 to 1000 nm. The spectrum consisted of two peaks: 560 nm (approx) and 800 nm (approx). The purity of AuNBPs in solution was calculated from comparing the LSPR absorbance peak to the spherical impurity absorbance peak. TEM images were used to quantify the purity.

Optimization of Yield from Unheated Seed-Mediated Growth Methods. To optimize the yield of AuNBPs made from unheated seeds, different concentrations of DMAB, HCl, and $AgNO_3$ were added to the reaction mixture. For DMAB optimization, 0.025, 0.05, 0.1, 0.2, and 0.3 M concentrations were used, keeping every other concentration and condition same. For HCl optimization, 0, 20, 40, 80, 120, and 200 μL of 1 N HCl were added in different reaction mixtures. Different centrifugation−resuspension conditions following AuNBP growth, including RPM, centrifugation time, and DMAB concentration after resuspension, were also optimized. LSPR wavelength of AuNBPs can be tuned by altering the aspect ratio of AuNBPs. The aspect ratio of NBPs is governed by the seed concentration in the growth solution. To tune LSPR in the NIR region, seed volume was increased from 60 to 140 μL in steps of 20 μL.

Increasing DMAB-AuNBPs Yield with BDAC Flocculation. BDAC was added to AuNBPs in solution to flocculate and precipitate the particles to increase purity following removal of the supernatant and resuspension. The growth solution was centrifuged at 5000 rpm for 10 min. The pellet was resuspended in 4 mL of 0.01 M DMAB. The process was repeated twice to wash the pellet. The pellet was resuspended in 1.2 mL of 10 mM DMAB. Then 2.56 mL of BDAC (0.5 M) was added to the tube containing 1.2 mL of nanostructure solution, and the volume was made 4 mL by adding 240 μL of water. The mixture was mixed well and left undisturbed for 16 h at 30 °C. The pink supernatant was removed, and 1.2 mL of 10 mM DMAB was added to the precipitate. The tube was sonicated for 2 min. The resulting purified solution (brownish in color) was centrifuged at 5000 rpm for 10 min. The supernatant was discarded and replaced with 1 mL of 10 mM DMAB. The step was repeated twice to remove the BDAC completely from the solution. The purified bipyramids were redispersed in 600 μL of 10 mM DMAB. The yield of NBPs was determined by UV−vis spectroscopy.

Phototransduction, in Vitro Biocompatibility, and Cancer Theranostics Studies: Gold concentration in synthesized NBPs was determined by inductively coupled plasma−atomic emission spectroscopy (ICP-AES). Different dilutions of samples were made. The samples were loaded in 96-well plate, and the plate was kept floating in a water bath at a constant temperature of 37 °C. The NIR laser (808 nm, 2 W/cm^2) was irradiated on each well for different times (1, 2, 3, 4, and 5 min), and the temperature of the samples was noted. Two $\times 10^5$ L929 normal cells were used to evaluate cell viability, followed by the (3-[4,5-dimethylthiazol-2-yl]-2,5 diphenyl tetrazolium bromide) (MTT) assay. DMAB and CTAB-decorated AuNBPs were tested with normal cells at various concentrations (5−500 ug/mL). During this assay, cells were incubated for 24 h with 5% CO_2 in Dulbecco's Modified Eagle's Medium (DMEM Gibco, Carlsbad, CA, USA) and supplemented with 10% fetal bovine serum and penicillin/streptomycin at 37.0 °C. After complete incubation, engineered nanoparticles were treated with cells for overnight with 100 μL of each nanoparticle (5 to 500 ug/mL). These cells were washed with PBS to remove excess particles from the treatment. Now, 20 μL of MTT dye was added to estimate the % cell viability, where formazan crystals were dissolved using 180−200 μL of dimethyl sulfoxide (DMSO). The optical absorbance was recorded using microplate reader (Tecan Infinite 200 PRO). Cells without nanoparticle treatment were considered a control for calculating the % cell viability from the MTT assay. The cancer theranostic performance of engineered nanoparticles was evaluated on breast cancer cells. MDA-MB231 breast cancer cells (2×10^5 cells/well) were cultured and treated with DOX-loaded DMAB-stabilized AuNBPs with and without NIR light (808 nm, 2 W/cm^2). Prior to beginning the cancer therapeutics, 100 μL of drug-loaded nanoparticles were treated with breast cancer cells for 4 h, and then these treated cancer cells were washed with PBS to remove the unattached nanoparticles. Then 20 μL of MTT dye was added to estimate the % cell viability, where formazan crystals were dissolved using 180−200 μL of DMSO. The optical absorbance was recorded using microplate reader (Tecan Infinite 200 PRO).

Cancer Cell Imaging and Molecular GSH Detection. For cell imaging, breast cancer cells were treated with red emitting (due to DOX) AuNBPs (100 μL) and incubated for 4 h. Now, these cells were washed with PBS thoroughly, fixed with 4% paraformaldehyde, and stained with 4,6-diamidino-2-phenylindole (DAPI for cell nuclei). These treated and stained cells were mounted with the coverslip using 70% glycerol on a glass slide and then brought under a fluorescence microscope to track the location of red dots (from DOX-loaded AuNBPs) and blue nuclei, whereas for molecular GSH detection, 0.5 mL of as-synthesized AuNBPs were mixed with 1 mL of growth solution. Different concentrations of glutathione were added to AuNBPs, and a change in color was observed. The UV−vis spectra were taken at different intervals of time. Morphological change was visualized using HR-TEM (300 keV).

Quantification and Statistical Analysis. All experiments were performed in technical triplicate. Error bars represent standard deviation unless otherwise noted. Cell viability experiments were also performed in technical triplicate to enable calculation of standard deviation. Data were analyzed and plotted using OriginPro 8 and Graphpad Prism software. Graphpad Prism was also used to perform statistical analysis such as error calculations and Student *t* tests where appropriate.

■ ASSOCIATED CONTENT

Supporting Information

The Supporting Information is available free of charge at https://pubs.acs.org/doi/10.1021/acsabm.4c00409.

UV−vis spectra and TEM images of the starting Au seeds; the longitudinal diameters of DMAB-AuNBPs and CTAB-AuNBPs were calculated from TEM images following manual segmentation; UV−vis spectra of DMAB-AuNBPs were characterized following BDAC-mediated flocculation purification; The photothermal profile of DMAB-AuNBPs in solution was characterized as a function of time and AuNBP concentration; UV−vis spectra of DMAB-AuNBPs in different concentrations of GSH over time were evaluated (PDF)

■ AUTHOR INFORMATION

Corresponding Authors

Rajendra Prasad − *School of Biochemical Engineering, Indian Institute of Technology (BHU), Varanasi, Uttar Pradesh 221005, India;* orcid.org/0000-0001-9851-8630; Email: rajendra.bce@iitbhu.ac.in

Rohit Srivastava − *Department of Biosciences and Bioengineering, Indian Institute of Technology Bombay,*

https://doi.org/10.1021/acsabm.4c00409
ACS Appl. Bio Mater. 2024, 7, 4542−4552

Powai, Mumbai 400076, India; orcid.org/0000-0002-3937-5139; Email: rsrivasta@iitb.ac.in

Pranjal Chandra − *School of Biochemical Engineering, Indian Institute of Technology (BHU), Varanasi, Uttar Pradesh 221005, India;* orcid.org/0000-0003-3428-3195; Email: pranjal.bce@iitbhu.ac.in

Authors

Nishant Kumar Jain − *Department of Biosciences and Bioengineering, Indian Institute of Technology Bombay, Powai, Mumbai 400076, India;* orcid.org/0000-0002-1957-2581

Shubham Pallod − *Department of Biosciences and Bioengineering, Indian Institute of Technology Bombay, Powai, Mumbai 400076, India;* Present Address: Arizona State University, Biodesign Institute 1001 South McAllister Avenue, Tempe, Tempe, AZ, US 85287-1004; phone, (480)937-6132

Berney Peng − *Department of Pathology and Laboratory Medicine, University of California at Los Angeles, Los Angeles, California 90095, United States*

Rohini Kumari − *School of Biochemical Engineering, Indian Institute of Technology (BHU), Varanasi, Uttar Pradesh 221005, India*

Deepak Singh Chauhan − *Department of Biosciences and Bioengineering, Indian Institute of Technology Bombay, Powai, Mumbai 400076, India; Department of Microbiology and Immunology, Dalhousie University, Halifax, NS 6299, Canada; Department of Pediatrics, IWK Research Center, Halifax, Nova Scotia 6299, Canada*

Mukesh Dhanka − *Department of Biosciences and Bioengineering, Indian Institute of Technology Bombay, Powai, Mumbai 400076, India; Department of Biological Sciences and Engineering, Indian Institute of Technology, Gandhinagar 382055 Gujarat, India*

Eaint Honey Aung Win − *Department of Pathology and Laboratory Medicine, University of California at Los Angeles, Los Angeles, California 90095, United States*

Michael A. Teitell − *Department of Pathology and Laboratory Medicine, University of California at Los Angeles, Los Angeles, California 90095, United States;* orcid.org/0000-0002-4495-8750

Complete contact information is available at: https://pubs.acs.org/10.1021/acsabm.4c00409

Author Contributions

[$]R.P. and R.S. conceived the idea and designed the project. R.P., S.P., R.K. and N.K.J. have done major experiments in engineering nanoparticles, and their characterization. N.K.J, D.S.C., B.P. and E.H.A.W. have done in vitro testing. P.C., R.K., M.D. and M.A.T. have provided their critical input during this project. All authors have contributed to writing the draft and have approved the final version of the manuscript. These authors have contributed equally to this project.

Notes

The authors declare no competing financial interest.

■ ACKNOWLEDGMENTS

R.P. thanks the Director and the School of Biochemical Engineering, Indian Institute of Technology (BHU), Varanasi, for the support. P.C. acknowledges the ICMR grant (sanction letter no. R.11013/47/2021-GIA/HR) for providing financial support. We acknowledge the Sophisticated Analytical Instrumentation Facility (SAIF) at IIT Bombay for instrumentation support. This work was supported by the Department of Biotechnology, Government of India. M.A.T., E.H.A.W., and B.P. acknowledge support provided by the UCLA Tumor Immunology Institutional Training Grant from the National Institutes of Health, USA (NIH grant 2T32CA009120-46A1).

■ REFERENCES

(1) Hu, J. J.; Cheng, Y. J.; Zhang, X. Z. Recent advances in nanomaterials for enhanced photothermal therapy of tumors. *Nanoscale* **2018**, *10* (48), 22657−22672.

(2) Si, P.; Shevidi, S.; Yuan, E.; Yuan, K.; Lautman, Z.; Jeffrey, S. S.; Sledge, G. W.; de la Zerda, A. Gold Nanobipyramids as Second Near Infrared Optical Coherence Tomography Contrast Agents for in Vivo Multiplexing Studies. *Nano Lett.* **2020**, *20* (1), 101−108.

(3) Prasad, R.; Selvaraj, K. Effective Distribution of Gold Nanorods in Ordered Thick Mesoporous Silica: A Choice of Noninvasive Theranostics. *ACS Appl. Mater. Interfaces* **2023**, *15* (40), 47615−47627.

(4) Dahan, K. A.; Li, Y.; Xu, J.; Kan, C. Recent progress of gold nanostructures and their applications. *Phys. Chem. Chem. Phys.* **2023**, *25*, 18545−18576.

(5) Chow, T. H.; Li, N.; Bai, X.; Zhuo, X.; Shao, L.; Wang, J. Gold Nanobipyramids: An Emerging and Versatile Type of Plasmonic Nanoparticles. *Acc. Chem. Res.* **2019**, *52* (8), 2136−2146.

(6) Kumar, R.; Srivastava, V. R.; Mahapatra, S.; Dkhar, D. S.; Kumari, R.; Prerna, K.; Dubey, V. K.; Chandra, P. Drug Encapsulated Lipid-Polymeric Nanohybrid as a Chemo-therapeutic Platform of Cancer. *Nanotheranostics.* **2023**, *7* (2), 167−175.

(7) Borse, V.; Chandra, P.; Srivastava, R. *BioSensing, Theranostics, and Medical Devices: From Laboratory to Point-of-Care Testing*; Springer: Singapore, 2021.

(8) Chandra, P. Personalized biosensors for point-of-care diagnostics: from bench to bedside applications. *Nanotheranostics.* **2023**, *7* (2), 210−215.

(9) Chandra, P.; Prakash, R. . *Nanobiomaterial Engineering: Concepts and Their Applications in Bio-medicine and Diagnostics*; Springer: Singapore, 2020.

(10) Peng, B.; Almeqdadi, M.; Laroche, F.; Palantavida, S.; Dokukin, M.; Roper, J.; Yilmaz, O. H.; Feng, H.; Sokolov, I. Ultrabright fluorescent cellulose acetate nanoparticles for imaging tumors through systemic and topical applications. *Mater. Today (Kidlington).* **2019**, *23*, 16−25.

(11) Peng, B.; Almeqdadi, M.; Laroche, F.; Palantavida, S.; Dokukin, M.; Roper, J.; Yilmaz, O. H.; Feng, H.; Sokolov, I. Data on ultrabright fluorescent cellulose acetate nanoparticles for imaging tumors through systemic and topical applications. *Data Brief.* **2019**, *22*, 383−391.

(12) Vines, J. B.; Yoon, J. H.; Ryu, N. E.; Lim, D. J.; Park, H. Gold Nanoparticles for Photothermal Cancer Therapy. *Front Chem.* **2019**, *7*, 167.

(13) Faid, A. H.; Shouman, S. A.; Badr, Y. A.; Sharaky, M. Enhanced photothermal heating and combination therapy of gold nanoparticles on a breast cell model. *BMC Chem.* **2022**, *16*, 66.

(14) Abadeer, N. S.; Murphy, C. J. Recent Progress in Cancer Thermal Therapy Using Gold Nanoparticles. *J. Phys. Chem. C* **2016**, *120*, 4691−4716.

(15) Kang, Y. F.; Zheng, B.; Li, C. Y.; Zhang, Z. L.; Tang, H. W.; Wu, Q. S.; Pang, D. W. Real-Time Monitoring of Temperature Variations around a Gold Nanobipyramid Targeted Cancer Cell under Photothermal Heating by Actively Manipulating an Optically Trapped Luminescent Upconversion Microparticle. *Anal. Chem.* **2020**, *92* (1), 1292−1300.

(16) Wei, M. Z.; Deng, T. S.; Zhang, Q.; Cheng, Z.; Li, S. Seed-Mediated Synthesis of Gold Nanorods at Low Concentrations of CTAB. *ACS Omega.* **2021**, *6* (13), 9188−9195.

(17) Chapagain, P.; Guisbiers, G.; Kusper, M.; Geoffrion, L. D.; Benamara, M.; Golden, A.; Bachri, A.; Hewavitharana, L. Tuning the Surface Plasmon Resonance of Gold Dumbbell Nanorods. *ACS Omega.* **2021**, *6* (10), 6871−6880.
(18) Ye, Z.; Wang, Ke; Lou, M.; JIa, X.; Xu, F.; Ye, G. Consecutive synthesis of gold nanobipyramids with controllable morphologies using a microfluidic platform. *Microfluid. Nanofluid.* **2020**, *24*, 38.
(19) Liu, X.; Zhou, W.; Wang, T.; Miao, S.; Lan, S.; Wei, Z.; Meng, Z.; Dai, Q.; Fan, H. Highly localized, efficient, and rapid photothermal therapy using gold nanobipyramids for liver cancer cells triggered by femtosecond laser. *Sci. Rep.* **2023**, *13* (1), 3372.
(20) Wu, X.; Mu, L.; Chen, M.; Liang, S.; Wang, Y.; She, G.; Shi, W. Bifunctional gold nanobipyramids for photothermal therapy and temperature monitoring. *ACS Applied Bio Materials* **2019**, *2*, 2668−2675.
(21) Allen, J. M.; Xu, J.; Blahove, M.; Canonico-May, S. A.; Santaloci, T. J.; Braselton, M. E.; Stone, J. W. Synthesis of less toxic gold nanorods by using dodecylethyldimethylammonium bromide as an alternative growth-directing surfactant. *J. Colloid Interface Sci.* **2017**, *505*, 1172−1176.
(22) Navarro, J. R G; Manchon, D.; Lerouge, F.; Cottancin, E.; Lerme, J.; Bonnet, C.; Chaput, F.; Mosset, A.; Pellarin, M.; Parola, S. Synthesis, electron tomography and single-particle optical response of twisted gold nano-bipyramids. *Nanotechnology* **2012**, *23*, 145707.
(23) Fang, C.; Zhao, G.; Xiao, Y.; Zhao, J.; Zhang, Z.; Geng, B. Facile growth of high-yield gold nanobipyramids induced by chloroplatinic acid for high refractive index sensing properties. *Sci. Rep.* **2016**, *6*, 36706.
(24) Rao, W.; Li, Q.; Wang, Y.; Li, T.; Wu, L. Comparison of photoluminescence quantum yield of single gold nanobipyramids and gold nanorods. *ACS Nano* **2015**, *9* (3), 2783−2791.
(25) Chateau, D.; Liotta, A.; Vadcard, F.; Navarro, J. R. G.; Chaput, F.; Lermé, J.; Lerouge, F.; Parola, S. From gold nanobipyramids to nanojavelins for a precise tuning of the plasmon resonance to the infrared wavelengths: experimental and theoretical aspects. *Nanoscale* **2015**, *7*, 1934−1943.
(26) Jana, N. R.; Gearheart, L.; Murphy, C. J. Seed-mediated growth approach for shape-controlled synthesis of spheroidal and rod-like gold nanoparticles using a surfactant template. *Adv. Mater.* **2001**, *13* (18), 1389−1393.
(27) Murphy, C. J.; Thompson, L. B.; Chernak, D. J.; Yang, J. A.; Sivapalan, S. T.; Boulos, S. P.; Huang, J.; Alkilany, A. M.; Sisco, P. N. Gold nanorod crystal growth: from seed-mediated synthesis to nanoscale sculpting. *Curr. Opin. Colloid Interface Sci.* **2011**, *16*, 128−134.
(28) Hubert, F.; Testard, F.; Spalla, O. Cetyltrimethylammonium bromide silver bromide complex as the capping agent of gold nanorods. *Langmuir* **2008**, *24* (17), 9219−9222.
(29) Liu, M.; Guyot-Sionnest, P. Mechanism of silver (I)-assisted growth of gold nanorods and bipyramids. *J. Phys. Chem. B* **2005**, *109* (47), 22192−22200.
(30) Li, Q.; Zhuo, X.; Li, S.; Ruan, Q.; Xu, Q. H.; Wang, J. Production of monodisperse gold nanobipyramids with number percentages approaching 100% and evaluation of their plasmonic properties. *Advanced Optical Materials* **2015**, *3* (6), 801−812.
(31) Lee, J. H.; Gibson, K. J.; Chen, G.; Weizmann, Y. Bipyramid-templated synthesis of monodisperse anisotropic gold nanocrystals. *Nat. Commun.* **2015**, *6*, 7571.
(32) Qi, Y.; Zhu, J.; Li, J.; Zhao, J. Highly improved synthesis of gold nanobipyramids by tuning the concentration of hydrochloric acid. *J. Nanopart. Res.* **2016**, *18*, 190.
(33) Sánchez-Iglesias, A.; Winckelmans, N.; Altantzis, T.; Bals, S.; Grzelczak, M.; Liz-Marzán, L. M. High-yield seeded growth of monodisperse pentatwinned gold nanoparticles through thermally induced seed twinning. *J. Am. Chem. Soc.* **2017**, *139* (1), 107−110.
(34) Fahimi-Kashani, N.; Shadabipour, P.; Hormozi-Nezhad, M. R. Colorimetric detection of glutathione based on transverse overgrowth of high aspect ratio gold nanorods investigated by MCR-ALS. *RSC Adv.* **2015**, *5* (101), 82906−82915.
(35) Sudeep, P. K.; Joseph, S. S.; Thomas, K. G. Selective detection of cysteine and glutathione using gold nanorods. *J. Am. Chem. Soc.* **2005**, *127* (18), 6516−6517.
(36) Gamcsik, M. P.; Kasibhatla, M. S.; Teeter, S. D.; Colvin, O. M. Glutathione levels in human tumors. *Biomarkers* **2012**, *17* (8), 671−691.
(37) Hendel, T.; Wuithschick, M.; Kettemann, F.; Birnbaum, A.; Rademann, K.; Polte, J. In situ determination of colloidal gold concentrations with UV-vis spectroscopy: limitations and perspectives. *Anal. Chem.* **2014**, *86* (22), 11115−24.
(38) Liu, Q.; Liu, H.; Sacco, P.; Djaker, N.; Lamy de la Chapelle, M.; Marsich, E.; Li, X.; Spadavecchia, J. CTL-doxorubicin (DOX)-gold complex nanoparticles (DOX-AuGCs): from synthesis to enhancement of therapeutic effect on liver cancer model. *Nanoscale Adv.* **2020**, *2* (11), 5231−5241.
(39) Manivasagan, P.; Bharathiraja, S.; Bui, N. Q.; Jang, B.; Oh, Y. O.; Lim, I. G.; Oh, J. Doxorubicin-loaded fucoidan capped gold nanoparticles for drug delivery and photoacoustic imaging. *Int. J. Biol. Macromol.* **2016**, *91*, 578−88.
(40) Prasad, R.; Jain, N. K.; Yadav, A. S.; Jadhav, M.; Radharani, N. N. V.; Gorain, M.; Kundu, G. C.; Conde, J.; Srivastava, R. Ultrahigh penetration and retention of graphene quantum dot mesoporous silica nanohybrids for image guided tumor regression. *ACS Applied Bio Materials* **2021**, *4* (2), 1693−1703.
(41) Du, Y.; Xia, L.; Jo, A.; Davis, R. M.; Bissel, P.; Ehrich, M. F.; Kingston, D. G. I. Synthesis and Evaluation of Doxorubicin-Loaded Gold Nanoparticles for Tumor-Targeted Drug Delivery. *Bioconjug Chem.* **2018**, *29* (2), 420−430.
(42) Faid, A. H.; Shouman, S. A.; Badr, Y. A.; Sharaky, M. Enhanced cytotoxic effect of doxorubicin conjugated gold nanoparticles on breast cancer model. *BMC Chemistry* **2022**, *16*, 90.

https://doi.org/10.1021/acsabm.4c00409
ACS Appl. Bio Mater. 2024, 7, 4542−4552